It must be pointed out that the present results apply only to the case of atoms in general positions and, like most conventional statistical tests, they do not overcome the problems of possible hypersymmetry. In the case of light-atom hypersymmetric structures, use can be made of the cumulative distributions given by Lipson & Woolfson (1952) and Rogers & Wilson (1953) (*cf.* Goldberg & Shmueli, 1973), while for the case of outstandingly heavy atoms modified probability density functions and/or modified expressions for the higher moments of $|E|$ are required.

It should also be pointed out that the more extensive validity of the Wilson-type methods (more extensive than their underlying assumptions might lead one to expect) is probably due in part to the decrease of the correction terms in (14)–(17) with increasing symmetry. This is indicated by the above example and may account for numerous successful outcomes of $N(z)$ tests (Howells *et al.*, 1950) carried out with moderately heavy atoms.

References

ABRAMOVITZ, M. & STEGUN, I. (1970). Editors. *Handbook of Mathematical Functions*. New York: Dover.

BERTAUT, E. F. (1955). *Acta Cryst.* **8**, 823–832.

FOSTER, F. & HARGREAVES, A. (1963*a*). *Acta Cryst.* **16**, 1124–1133.

FOSTER, F. & HARGREAVES, A. (1963*b*). *Acta Cryst.* **16**, 1133–1139.

GOLDBERG, I. & SHMUELI, U. (1971). *Acta Cryst.* B**27**, 2164–2173.

GOLDBERG, I. & SHMUELI, U. (1973). *Acta Cryst.* B**29**, 440–448.

HAUPTMAN, H. & KARLE, J. (1953*a*). *Acta Cryst.* **6**, 136–141.

HAUPTMAN, H. & KARLE, J. (1953*b*). *Solution of the Phase Problem. I. The Centrosymmetric Crystal.* ACA Monograph No. 3.

HOCHSTRASSER, U. W. (1970). *Handbook of Mathmetical Functions*, edited by M. ABRAMOVITZ & I. STEGUN, p. 801. New York: Dover.

HOWELLS, E. R., PHILLIPS, D. C. & ROGERS, D. (1950). *Acta Cryst.* **3**, 210–214.

KARLE, I. L. (1976). *Crystallographic Computing Techniques*, edited by F. R. AHMED, p. 29. Copenhagen: Munksgaard.

KARLE, J. & HAUPTMAN, H. (1953). *Acta Cryst.* **6**, 131–135.

LIPSON, H. & WOOLFSON, M. M. (1952). *Acta Cryst.* **5**, 680–682.

ROGERS, D. & WILSON, A. J. C. (1953). *Acta Cryst.* **6**, 439–449.

SRINIVASAN, R. & PARTHASARATHY, S. (1976). *Some Statistical Applications in X-ray Crystallography*. Oxford: Pergamon Press.

WILSON, A. J. C. (1949). *Acta Cryst.* **2**, 318–321.

Acta Cryst. (1979). A**35**, 286–295

High-Resolution Diffuse X-ray Scattering Study from Nearly Perfect Silicon Single Crystals

BY KRISHAN LAL, BHANU PRATAP SINGH AND AJIT RAM VERMA

National Physical Laboratory, Hillside Road, New Delhi-110012, *India*

(*Received* 4 *July* 1978; *accepted* 12 *September* 1978)

Abstract

High-resolution measurements of diffuse X-ray scattering (DXS) have been made at and above room temperature around 111, 333, 444 and 555 reciprocal lattice points (relps) using highly collimated Mo $K\alpha_1$ and Cu $K\alpha_1$ radiations with the specimen set in $(1, -1, 1)$ symmetrical Bragg geometry. The distribution of DXS intensity around different relps has shown that at temperatures up to at least 573 K the contribution of thermal DXS to the observed DXS is very small. This is apparently due to the high value of the Debye temperature (640 K) of silicon. A remarkable feature of these results is that for the same value of the scattering vector $|\mathbf{K}^*|$ the DXS intensity is different for the parallel and antiparallel orientations of $\mathbf{K}^*$ relative to $\mathbf{R}^*$. The amount of anisotropy varied from sample to sample and depended on the thermal history of the specimen. This and the other features show that the observed DXS is predominantly due to point defects and their aggregates. A typical size parameter for the aggregates is 3000 to 10 000 Å.

1. Introduction

Point defects, their aggregates and elastic thermal waves give diffuse X-ray scattering (DXS) from regions of reciprocal space close to the reciprocal-

0567-7394/020286-10$01.00

© 1979 International Union of Crystallography

lattice point (relp). In principle, a study of DXS can give information about strain fields produced by defects and their clusters and therefore about defects themselves (Spalt, Lohstoler & Peisl, 1973; Larsen & Schmatz, 1974; Peisl, 1975). From the study of DXS due to elastic thermal waves, elastic constants (James, 1948; Ramachandran & Wooster, 1951*a*,*b*; Wooster, 1962; Phatak, Srivastava & Subbarao, 1972; Chandra & Hemkar, 1973) and phonon spectra of the crystal (Walker, 1956) can be obtained.

Experimentally, the use of conventional techniques (Wooster, 1962) involves a large number of uncertainties. Therefore, in recent years a number of attempts have been made to develop new techniques of measurement of DXS (Eisenberger, Alexandropoulos & Platzman, 1972; Larsen & Schmatz, 1974; Lal & Singh, 1977; Lal, 1977; Lal & Singh, 1978*a*; Lal, Singh & Verma, 1978). Recently, we have developed a high-resolution technique for the measurement of DXS (Lal, 1977; Lal & Singh, 1977, 1978*a*,*b*; Lal, Singh & Verma, 1978). In this technique a triple-crystal X-ray diffractometer (Lal & Singh, 1978*a*) in the (1,−1,1) configuration is used. In this paper we report the results of detailed investigations of DXS from dislocation-free silicon single crystals using this technique.

Silicon crystals are of interest because of their wide applications in semiconductor-device technology and also because of the following factors. It is now well established that in melt-grown crystals not all the vacancies present at the freezing point in the crystal are able to move out to the surface as the crystal is cooled to room temperature. These vacancies aggregate into clusters. Moreover, the background impurities and oxygen can also exist in aggregated form. DXS measurements were made on silicon by Prasad & Wooster (1955) to deduce the values of its elastic constants. However, the resolution of their technique was not as high as that attainable in the present technique. Moreover, some measurements of DXS on Si have been reported recently by Patel (1975). Most of the results reported in this paper are for measurements made around the 111 relp at room temperature. However, some measurements have been made around higher-order reflections: 333, 444, and 555. Results of some measurements made at temperatures above room temperature are also reported.

2. Experimental

(i) *Preparation of samples*

The specimen crystals used in this investigation were dislocation-free silicon single crystals; these were provided by Dr G. H. Schwuttke. The specimen crystals are cut parallel to the desired set of lattice planes and are ground and lapped (for use in the symmetrical Bragg configuration). To remove the surface damage a layer a few microns thick is etched from the surface of the specimen crystal in a nonpreferential etchant (CP4). If the diffraction curve of the as-etched specimen was found to be broad it was repeatedly etched until a narrow diffraction curve was obtained.

(ii) *Experimental set-up*

DXS measurements have been made on a triple-crystal X-ray diffractometer (Lal & Singh, 1977). We briefly describe the salient features of this instrument; further details will be published elsewhere. Fig. 1 shows a schematic line diagram of the experimental arrangement used in this investigation. This set-up essentially consists of (1) a monochromating stage and (2) a specimen-aligning arrangement. The monochromating stage consists of a turntable, two monochromator crystals and two collimators. The specimen-aligning arrangement consists of a special turntable, a goniometer head and a scintillation counter. The X-ray beam is collimated and monochromated by using Bonse monochromator crystals (Bonse & Hart, 1965). These are dislocation-free silicon single crystals cut parallel to (111) from the same crystal block. Monochromator crystals ($M1$ and $M2$) are mounted on a standard goniometer head and then mounted on a turntable in the (1, −1) setting. The X-ray beam from the source passes through a collimator and falls on the first monochromator. The monochromator crystals are able to resolve $K\alpha_1$ and $K\alpha_2$ components of the characteristic radiation when a point-focus source (40 μm diameter on the anode) is used. The $K\alpha_1$ beam is separated from the residual direct beam by a slit system. This $K\alpha_1$ beam is used as the exploring beam for the specimen crystal. The specimen crystal is mounted either on a standard two-arc goniometer or on a goniometer specially designed for the study of DXS at higher temperatures. The crystal-carrying goniometer is mounted on a special turntable. This can provide rotations of 1″ of arc to the crystal around the vertical axis. A scintillation counter is used as detector; it has a NaI (Tl) crystal as scintillator and an EMI-13 dynode photomultiplier (Type 9514 B). The output of this detector is fed into a counting system consisting of a linear amplifier, a single-channel analyser, a timer and a scaler.

It is well known that the intensity of DXS is very low compared to that of the direct X-ray beam and to that

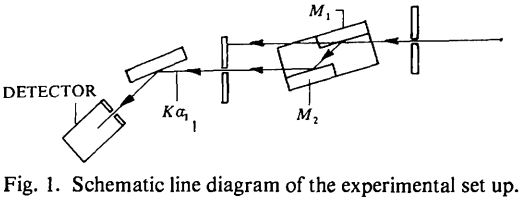

Fig. 1. Schematic line diagram of the experimental set up.

of the Bragg diffracted beam. Therefore, it is to be measured with great care. We know (Klug & Alexander, 1954) that if N_T is the total number of counts recorded in time t when the specimen and detector are set for a particular $\mathbf{K}^*$ ($\mathbf{K}^*$ is a vector from the nearest relp to the centre of the volume element in reciprocal space under investigation) and N_B is the number of background counts in the same time the probable error u_p (%) is given by

$$u_p = \frac{1{\cdot}64}{(R-1)}\left[\frac{R(R+1)}{N_T}\right]^{1/2}$$

for a 90% confidence level (here, $R = N_T/N_B$). For $u_p = 1\%$, this reduces to

$$N_T = 26896\,\frac{R(R+1)}{(R-1)^2}.$$

For a signal-to-background ratio of 1·1, N_T is of the order of 10^6 in order to give 1% probable error in the measured intensity for a 90% confidence level. Keeping this criterion in mind, counts are accumulated in the scaler for several hundred seconds. Values are noted after an interval of 50 s. The crystal is set for each value of $\mathbf{K}^*$ and the DXS intensity measured in the above fashion at least twice. This ensures the precision in the measured data. The data are analysed by using standard statistical methods. The error bars shown in the curves correspond to a confidence level of 90%.

(iii) *Resolution*

It is a convention to express the resolution of the DXS measurements in terms of the solid angle Ω subtended by the slit in front of the detector at the specimen crystal. It is implicit in this approach that (1) the exploring X-ray beam is strictly parallel and monochromatic and (2) the irradiated area of the specimen crystal is infinitesimally small (particularly that its width in the horizontal plane is very small). However, in practice there is a considerable spread in the wavelength and direction of the exploring beam, and the irradiated area of the specimen is finite. These factors have not received adequate attention in the past; however, they lead to a considerable loss of resolution (Lal & Singh, 1978*b*). We shall now describe the effect of these parameters on the resolution attainable with our equipment.

Because of finite wavelength spread the radius of the Ewald sphere will range from $1/\lambda_2$ to $1/\lambda_1$ where λ_1 and λ_2 are the shortest and longest wavelengths in the exploring X-ray beam. Because of finite direction spread in the exploring beam, the direction of the diameter of the Ewald sphere which defines the direction of the exploring beam is ill defined. Its uncertainty is equal to the direction spread of the exploring beam. These two factors lead to blurring of the reciprocal space and lead to uncertainty in the location of a relp.

We have measured experimentally the wavelength spread in the Mo $K\alpha_1$ exploring beam and also its direction spread. The uncertainty in the location of a reciprocal-lattice point due to wavelength and direction spread has been found to be about $3{\cdot}7 \times 10^3$ cm^{-1} in $\mathbf{K}^*$ space in our experimental set-up (Lal & Singh, 1978*b*). In contrast, the uncertainty in locating reciprocal-space points becomes more than 2×10^5 cm^{-1} for other existing instruments when Mo $K\alpha$ and not Mo $K\alpha_1$ radiation is used.

As mentioned above the irradiated area of the specimen, particularly the width of the exploring X-ray beam in the horizontal plane, should be infinitesimally small. This is because the detector receives the projected image of the irradiated area of the specimen. We have determined the resolution attainable in the present technique by performing a series of experiments in which the irradiated area and the solid angle Ω have been varied. The width of the exploring beam was varied from 15 to 65 μm. DXS experiments were also performed for the following exploring-beam heights: 1, 2, 4, 8 and 25 mm. From the DXS intensity *vs* $\mathbf{K}^*$ curves it was found that the nature of the curve remains unchanged for exploring-beam heights of 1 to 8 mm and that there is not much loss of resolution. Since we are measuring DXS intensity which is very small as compared to Bragg intensity we should optimize the experimental parameters in such a way that the exploring-beam intensity is as large as it can be without affecting resolution. Keeping this in mind we have kept the exploring-beam dimensions at 40 μm × 4 mm for most of our DXS measurements.

In another series of experiments we have made DXS measurements by varying Ω. In one experiment DXS measurements were made for the following widths of the slit in front of the detector: 0·08, 0·8 and 8·5 mm. In these experiments the specimen-to-detector distance was kept fixed at 180 mm. A plot of DXS intensity *vs* $\mathbf{K}^*$ shows that there is not much qualitative change in the nature of the curve. However, we have kept the receiving-slit width at 80 μm in most of the DXS measurements. It may be mentioned that the width of the detector slit is dependent on the width of the exploring X-ray beam. The slit width at the detector should, in principle, be equal to the width of the exploring beam. Decreasing the width of the slit in front of the detector to a value less than that of the exploring beam will lead to erroneous results. We have also performed experiments to determine the effect of the sample-to-detector slit distance on DXS measurements. This is another way of changing Ω. The experiments were performed for the following distances: 180 and 520 mm. The plot of DXS intensity *vs* $1/\mathbf{K}^{2*}$ shows that both curves have practically the same nature. Therefore, we have used a sample-to-detector

slit distance of 180 mm in most of our DXS measurements.

3. Relation between K* and the angular settings of the crystal and detector

In the DXS measurements one measures the intensity as a function of **K***. **K*** is a scattering vector which can be a wave vector of an elastic thermal wave or a displacement field vector caused by point defects or their aggregates in the lattice. The crystal and detector are mis-set from the exact Bragg diffraction condition to align the crystal for a specific **K***. Therefore, one requires a quantitative relation between **K*** and the angle of mis-set for the crystal (α) and the angle of mis-set for the detector ($\Delta\varphi$). When α and $\Delta\varphi$ are of the order of degrees, a graphical method can be successfully used (Ramachandran & Wooster, 1951*a*; Wooster, 1962). However, when the values of α and $\Delta\varphi$ are of the order of a few seconds of arc (as is the case in our investigation), the graphical method cannot be used. Until now approximate methods have been used for this purpose. We have developed an analytical method which correlates α and $\Delta\varphi$ with **K***. We shall now briefly describe this method for the general case when **K*** is inclined at an arbitrary angle to the reciprocal-lattice vector (rel vector) **R***.

Fig. 2 shows part of the intersection of the Ewald sphere with a horizontal plane passing through its centre *I*. *I* is also taken as the origin of the Cartesian coordinates. *O* is the origin of the reciprocal space and *P* is the relp under consideration so that $\overrightarrow{OP} = \mathbf{R}^*$. Let $\mathbf{K}^*$ ($= \overrightarrow{PP_1}$) be inclined at an angle ψ with $\mathbf{R}^*.P_1$ is brought on the Ewald sphere by suitably rotating the crystal and the detector from their positions corresponding to Bragg diffraction from the relp *P*.

The equation of line *OP* can be written as:

$$y(1 - \cos\varphi_0) + \sin\varphi_0 x = R\sin\varphi_0. \qquad (1)$$

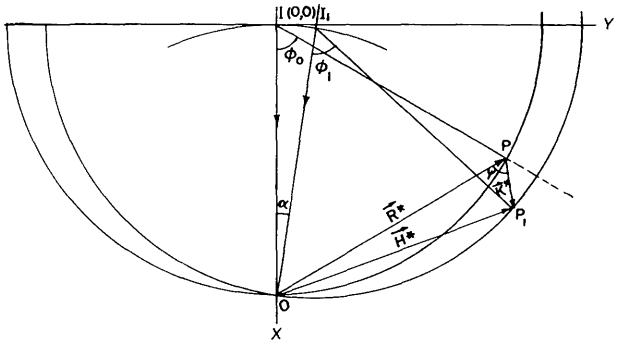

Fig. 2. Part of the intersection of the Ewald sphere with the horizontal plane.

Here $R = 1/\lambda$ = radius of the Ewald sphere; θ_B = Bragg angle and $\varphi_0 = 2\theta_B$. Let α be the angle of mis-set of the crystal to bring P_1 on the Ewald sphere. I_1 (in Fig. 2) is the centre of the Ewald sphere after this rotation; it has coordinates $[R\{1 - \cos\alpha\}, R\sin\alpha]$. The cross section of the Ewald sphere with the horizontal plane through II_1 is a circle. The equation of the circle with centre I_1 is

$$[x - R\{1 - \cos\alpha\}]^2 + [y - R\sin\alpha]^2 = R^2. \qquad (2)$$

Let the equation of the line PP_1 be given by

$$y = mx + c. \qquad (3)$$

Since we know the equation of the line *OP* [equation (1)] and the inclination of PP_1 to it ($= \psi$) the value of m can be easily determined. Similarly, c can be determined from the fact that PP_1 passes through *P*. From the intersection of the circle of equation (2) and the line of equation (3) we obtain the coordinates of P_1 (x_1, y_1) as:

$$x_1/R = \{(S_1 - mS_2) \pm [(S_1 - mS_2)^2 - (1 + m^2)(S_1^2 + S_2^2 - 1)]^{1/2}\}(1 + m^2)^{-1}$$

$$y_1 = mx_1 + c. \qquad (4)$$

Here $S_1 = 1 - \cos(\alpha)$, and $S_2 = (c/R) - \sin(\alpha)$. Equation (4) has two solutions for x_1 and y_1. Only those values of x_1 and y_1 which are close to the values of the coordinates of the relp P ($R\cos\varphi_0$, $R\sin\varphi_0$) are used in further calculations.

From the coordinates of P_1 [equation (4)], we can determine the direction cosines of $P_1 I_1$ as:

$$\left[\frac{x_1}{R} + \cos\alpha - 1\right], \left[\frac{y_1}{R} + \sin\alpha\right].$$

The direction cosines of OI_1 are $\cos\alpha$, $\sin\alpha$. Using these values of the direction cosines of $P_1 I_1$ and OI_1 we obtain

$$\varphi_1 = \angle P_1 I_1 O = \cos^{-1}\left[\cos\alpha\left\{\frac{x_1}{R} + \cos\alpha - 1\right\} + \sin\alpha\left\{\frac{y_1}{R} + \sin\alpha\right\}\right]. \qquad (5)$$

The angular mis-setting for the detector $\Delta\varphi = (\varphi_1 - \varphi_0)$ can be determined from equation (5). The length PP_1 is:

$$PP_1 = [(x_1 - R\cos\varphi_0)^2 + (y_1 - R\sin\varphi_0)^2]^{1/2}. \qquad (6)$$

From equations (5) and (6) we know the value of $|\mathbf{K}^*|$ for given values of $\bar{\alpha}$ and $\Delta\varphi$ when **K*** is inclined to **R*** at an arbitrary angle ψ.

4. Results and discussion

Measurements made around the 111 *relp*

Fig. 3 shows a typical diffraction or rocking curve for the 111 relp of a (111) dislocation-free silicon single crystal recorded in the (1,−1,1) setting. Mo $K\alpha_1$ radiation has been used as the exploring X-ray beam. The half-width of this curve is 5″ of arc, which is close to the theoretically expected half-width of this reflection for the Mo $K\alpha_1$ beam. Since this diffraction curve is very narrow we can make DXS measurements very close to the relp, *i.e.* for very small values of $|\mathbf{K}^*|$. DXS measurements can also be made at small intervals of $|\mathbf{K}^*|$.

Fig. 4 shows a typical plot of intensity of DXS (I) as a function of $1/\mathbf{K}^{*2}$ for measurements around the 111 relp and for $\mathbf{K}^*$ along [111], [$\bar{1}\bar{1}\bar{1}$], [0$\bar{1}$1] and [01$\bar{1}$]. We have chosen an I *vs* $1/K^{*2}$ plot because this plot is expected to be a straight line whether the observed DXS is due to elastic thermal waves or point defects [Huang scattering (Dederichs, 1971)]. The intensity of DXS due to thermal elastic waves is given by (James, 1948; Ramachandran & Wooster, 1951*a*; Wooster, 1962);

$$I = \frac{kT}{\tau} |F_T|^2 \frac{H^{*2}}{K^{*2}} K(f)_g. \qquad (7)$$

Here $\mathbf{H}^* = \mathbf{R}^* \pm \mathbf{K}^*$, $\mathbf{R}^*$ = rel vector; F_T = the structure factor for the relp under investigation corrected for temperature, k = Boltzmann's constant; T = temperature of measurements in K; τ = volume of the unit cell; and $K(f)_g$ is known as the rekha constant (Wooster, 1962) and depends on the elastic constants c_{ik} of the crystal, the direction cosines (f_i) of the elastic thermal wave vector $\mathbf{K}^*$ and the direction cosines (g_i) of the rel vector ($\mathbf{R}^*$). $K(f)_g$ is a complicated function of f_i, g_i and c_{ik} but is considerably simplified when g_i and f_i are chosen along simple directions and when the crystal has high crystallographic symmetry; for the 111 relp of a cubic crystal and for $\mathbf{K}^*$ along [111] and [0$\bar{1}$1] it is given by:

$$K(111)_{111} = \frac{3}{(c_{11} + 2c_{12} + 4c_{44})},$$

$$K(0\bar{1}1)_{111} = \frac{1}{3c_{44}} + \frac{4}{3(c_{11} + c_{12} + 2c_{44})}.$$

It can be seen from the experimentally observed plots shown in Fig. 4 that, for a given $|\mathbf{K}^*|$, the DXS intensity is much higher for $\mathbf{K}^*$ along $\mathbf{R}^*$ ($\mathbf{K}^*$ along [111]) than for $\mathbf{K}^*$ at right angles to $\mathbf{R}^*$ ($\mathbf{K}^*$ along [0$\bar{1}$1]). The slope of the line in the I *vs* $1/K^{*2}$ plot for $\mathbf{K}^*$ parallel to $\mathbf{R}^*$ is much higher than the slope of the line for $\mathbf{K}^*$ perpendicular to $\mathbf{R}^*$. Moreover, the DXS intensity is not symmetrically distributed around the relp for any given direction of $\mathbf{K}^*$. For example, DXS intensity for the same value of $|\mathbf{K}^*|$ is higher when $\mathbf{K}^*$ is along [$\bar{1}\bar{1}\bar{1}$] than when $\mathbf{K}^*$ is along [111]. Similar behaviour is observed for $\mathbf{K}^*$ along [01$\bar{1}$] and [0$\bar{1}$1]. Fig. 5 shows iso-intensity plots for the results shown in

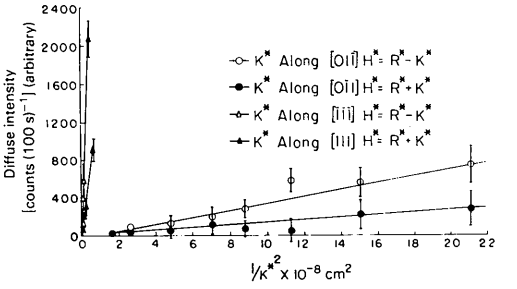

Fig. 4. A typical I *vs* $1/K^{*2}$ plot for the 111 relp of a (111) dislocation-free Si crystal. Mo $K\alpha_1$ radiation was used as the exploring beam; its diffraction curve is shown in Fig. 3.

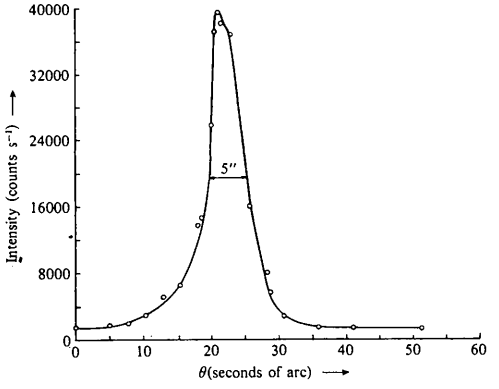

Fig. 3. A typical diffraction curve for the 111 relp of a (111) dislocation-free Si single crystal. Mo $K\alpha_1$ radiation was used as the exploring beam.

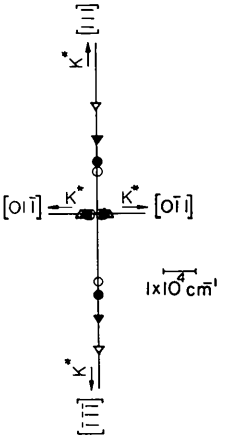

Fig. 5. A typical iso-intensity plot for the 111 relp of a (111) dislocation-free Si single crystal. Mo $K\alpha_1$ radiation was used as the exploring beam.

Fig. 4. It can be seen that even when **K*** is chosen along a particular direction, for a given value of $|\mathbf{K}^*|$, I is higher when θ is less than θ_B than when θ is greater than θ_B. This behaviour was found to depend on the sample under investigation. The anisotropy in intensity distribution was particularly large for **K*** parallel to **R***, *i.e.* **K*** along [111] and [$\bar{1}\bar{1}\bar{1}$].

We have performed experiments on a number of specimens. It was observed that even though the samples possess the same degree of perfection, as shown by the shape of their diffraction curves, the distributions of I around a relp may differ. In a recent paper (Lal & Singh, 1977) we reported an I *vs* $1/K^{*2}$ curve obtained from another sample. In this case, however, it was seen that for a given $|\mathbf{K}^*|$ value I is higher when $\theta > \theta_B$ than when $\theta < \theta_B$ for **K*** along [111].

Experiments have also been performed with Cu $K\alpha_1$ as the exploring X-ray beam. A typical I *vs* $1/K^{*2}$ plot and a typical diffraction curve are shown in Fig. 6(*a*) and (*b*) respectively. These results are similar to those obtained with Mo $K\alpha_1$ radiation on this sample.

The present results are remarkably different from those reported by Prasad & Wooster (1955). Therefore, we have attempted to discover the possible reasons for this discrepancy.

The minimum value of $|\mathbf{K}^*|$ used in the present investigation was about 2×10^3 cm^{-1} and no measurable DXS intensity was observed after the crystal was mis-set by about 1′ of arc from the exact Bragg diffraction condition. This corresponds to a $|\mathbf{K}^*|$ value of about 6×10^4 cm^{-1}. As mentioned in §2(i), long time intervals (~16 min) were used to record the DXS intensity for a given signal-to-background ratio so that the measured intensity lies within 1% of probable error.

The present results show that the observed DXS is not predominantly due to elastic thermal waves. If it were, the slope of the I *vs* $1/K^{*2}$ line in Figs. 4 and 6(*b*) for **K*** along [0$\bar{1}$1] should be higher than that of the line for **K*** along [111]. However, as can be seen in Figs. 4 and 6(*b*), the slopes are in the reverse order. This is rather surprising as Prasad & Wooster (1955) have deduced the values of elastic constants from DXS measurements of silicon single crystals at room temperature. The difference between our results and those of Prasad & Wooster may be due to the limited resolution of the conventional techniques (Lal & Singh, 1977, 1978*b*). With conventional single-crystal diffractometers the Bragg peaks have a half-width of about 1° of arc. The exploring beam in a conventional set-up has very high divergence and considerable wavelength spread. The data are recorded each time by mis-setting the crystal and detector by a degree of arc or so. Further, adequate attention is generally not paid to the perfection of the specimen crystal. In the 1950's, apparently, very perfect silicon single crystals were not available. Fig. 7 shows a typical diffraction curve of a KCl single crystal of ordinary perfection. This curve is spread over a degree of arc. At different settings of the crystal within the angular range of this curve different subgrains are set for diffraction. Therefore, what might be considered as DXS due to elastic thermal waves may actually be Bragg diffraction from misoriented subgrains.

We have also examined this discrepancy from a consideration of the energy of elastic thermal waves. We know that at thermodynamic equilibrium the energy

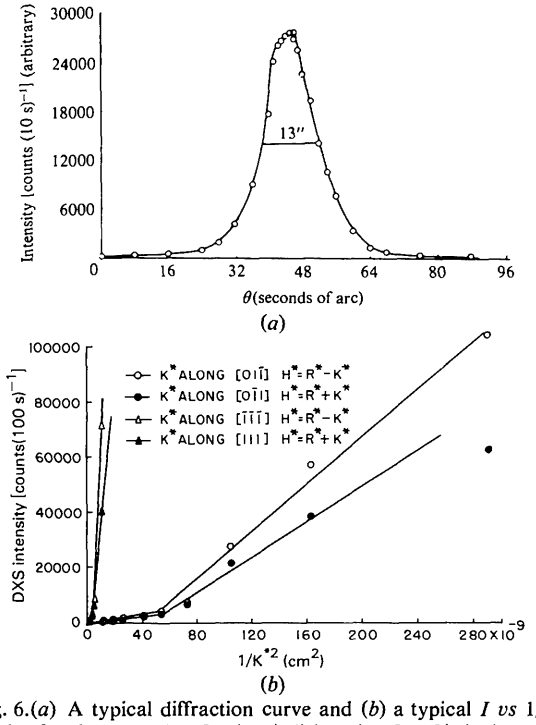

Fig. 6.(*a*) A typical diffraction curve and (*b*) a typical I *vs* $1/K^{*2}$ plot for the 111 relp of a (111) dislocation-free Si single crystal. Cu $K\alpha_1$ radiation was used as the exploring beam.

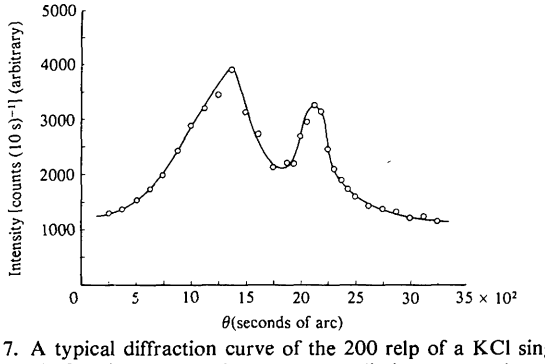

Fig. 7. A typical diffraction curve of the 200 relp of a KCl single crystal of ordinary perfection. Cu $K\alpha_1$ radiation was used as the exploring beam.

per elastic mode is equal to kT. This energy is proportional to the product of the square of the frequency $\nu_{(i)}$ and the amplitude of the elastic wave $\xi_{(i)}$ (Wooster, 1962): $kT = 2\pi m \nu_{(i)}^2 \xi_{(i)}^2$ (here m = mass of the unit cell). This means that at any temperature T, $\xi_{(i)}^2$ and hence the intensity of DXS due to elastic thermal waves is inversely proportional to $\nu_{(i)}^2$. In our investigation, the maximum $|\mathbf{K}^*|$ value is less than 6×10^4 cm^{-1}, which in terms of frequency is approximately 6×10^9 cycles s^{-1}. In the earlier work the maximum value of $|\mathbf{K}^*|$ is about 6×10^6 cm^{-1} so that the intensity is expected to be smaller by 10^4 than the DXS intensity observed in the present case for $|\mathbf{K}^*| = 6 \times 10^4$ cm^{-1}. This shows that it may not be feasible to see elastic thermal waves with such high values of $\mathbf{K}^*$ until X-ray sources of extremely high power are used. Moreover, the Debye temperature for Si is 640 K (*American Institute of Physics Handbook*, 1957). This is much higher than room temperature and it may be for this reason that we do not observe the contribution of elastic thermal waves to the DXS. It is expected to be small.

Measurements made around higher-order relps

As discussed above, the present results suggest that the observed DXS intensity is not predominantly due to elastic thermal waves. We have also made DXS measurements around the 333, 444 and 555 relps of (111) Si single crystals using Mo $K\alpha_1$ radiation as the exploring beam. Figs. 8(*a*), 9(*a*) and 10(*a*) show diffraction curves for the 333, 444 and 555 relps respectively. Figs. 8(*b*), 9(*b*) and 10(*b*) show plots of intensity of DXS I, as a function of $1/K^{*2}$ for the 333, 444 and 555 relps respectively. These measurements were made for $\mathbf{K}^*$ along [111], [$\bar{1}\bar{1}\bar{1}$], [0$\bar{1}$1] and [01$\bar{1}$]. The half-widths of the diffraction curves [Figs. 8(*a*), 9(*a*) and 10(*a*)] for these relps are much larger than those of the diffraction curve for the 111 relp (Fig. 3). The broadening of the peaks is expected to be due to dispersion as the crystals are set in the (1,−1,n) setting with $n = 3$, 4 and 5 for the 333, 444 and 555 reflections respectively. The broadening due to dispersion is expected to be

$$d\theta = \frac{d\lambda}{2d \cos\theta}. \qquad (9)$$

However, the observed broadening is much more than can be accounted for by dispersion. It seems that DXS is responsible for the broadening of the diffraction curves for higher-order reflections.

From the I *vs* $1/K^{*2}$ plots shown in Figs. 8(*b*), 9(*b*) and 10(*b*), it can be seen that these plots are not single straight lines. Each plot, in fact, consists of at least two

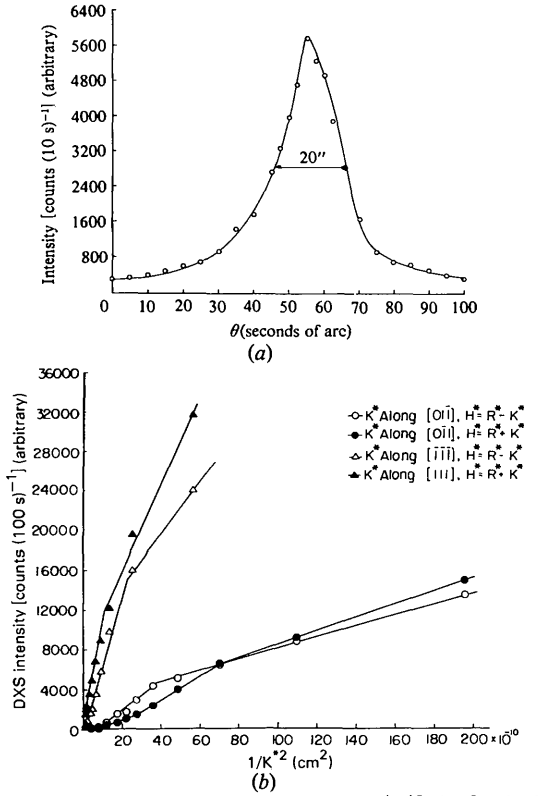

Fig. 8.(*a*) A diffraction curve and (*b*) an I *vs* $1/K^{*2}$ plot for the 333 relp of a (111) dislocation-free Si single crystal. Mo $K\alpha_1$ radiation was used as the exploring beam.

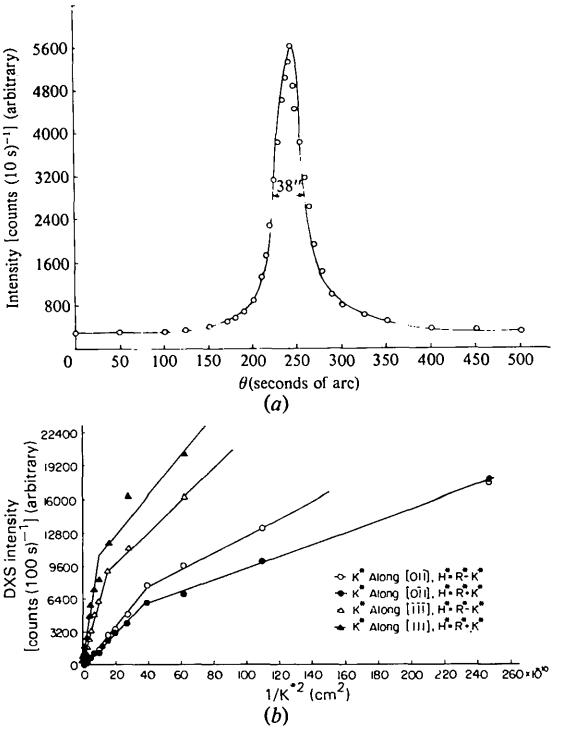

Fig. 9.(*a*) A diffraction curve and (*b*) an I *vs* $1/K^{*2}$ plot for the 444 relp of a (111) dislocation-free Si single crystal. Mo $K\alpha_1$ radiation was used as the exploring beam.

straight lines with different slopes. The slopes of the I *vs* $1/K^{*2}$ lines for **K*** parallel or antiparallel to [111] are much higher than those for the lines corresponding to **K*** parallel or antiparallel to $[0\bar{1}1]$ for the 333 and 444 relps [Figs. 8(*b*) and 9(*b*)]. This behaviour is in agreement with the DXS results obtained for the 111 relp [Figs. 4 and 6(*b*)].

A gradual change in the slope of the I *vs* $1/K^{*2}$ lines is observed as one goes from the 111 to the 555 relp. The slope of the I *vs* $1/K^{*2}$ line for **K*** parallel or antiparallel to $[0\bar{1}1]$ is nearly the same as that for **K*** parallel or antiparallel to [111]. Furthermore, like the DXS intensity around the 111 relp, the distribution of the DXS intensity is anisotropic for any particular direction of **K*** around these higher-order relps, the intensity being higher for $\theta > \theta_B$ than for $\theta < \theta_B$ for these relps. According to equation (7) one expects a change of slope of I *vs* $1/K^{*2}$ plots from reflection to reflection as $I/(1/K^{*2}) \propto H^{*2}$. In Table 1 we have given the values of slopes of different lines in the I *vs* $1/K^{*2}$ plots for the 111, 333, 444 and 555 relps. It can be seen that not only do the plots have more than one straight line but for higher-order relps the slopes do not change as H^{*2}. In fact, the slopes of the lines for **K*** along [111] or $[\bar{1}\bar{1}\bar{1}]$ decrease with increasing orders of reflection.

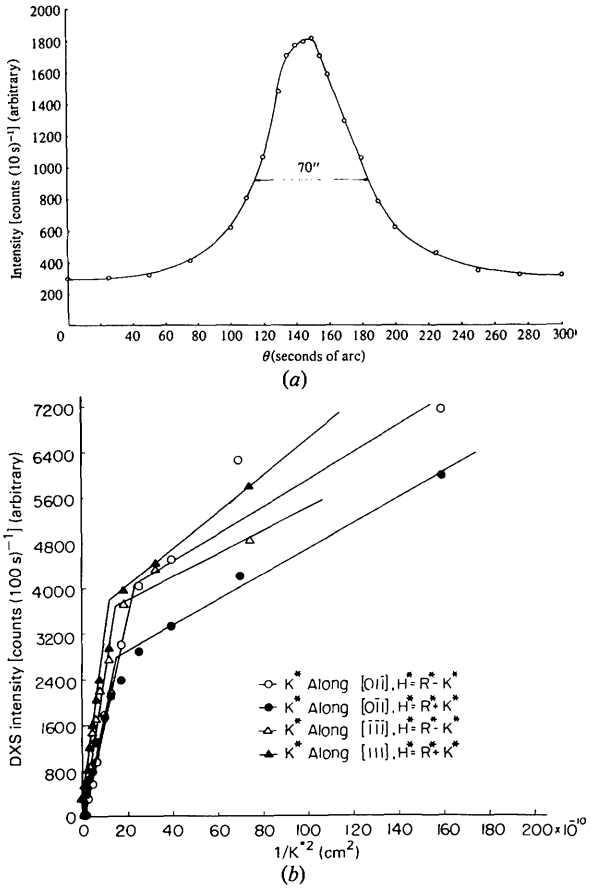

Fig. 10.(*a*) A diffraction curve and (*b*) an I *vs* $1/K^{*2}$ plot for the 555 relp of a (111) dislocation-free Si single crystal. Mo $K\alpha_1$ radiation was used as the exploring beam.

Measurements made at higher temperatures

Since the Debye temperature of silicon is much above room temperature we have made DXS measurements above room temperature. Cu $K\alpha_1$ radiation was used as the exploring beam. Measurements were made at 373, 473 and 573 K. No significant change in DXS intensity was observed up to 473 K. Also, the shape of the diffraction curve did not change significantly with increase in temperature up to 473 K. At 573 K an appreciable effect of temperature on the height of the diffraction curve, as well as on its width, is seen. The half-width of the diffraction curve is 13″ of arc when the specimen is at room temperature and 25″ of arc when the specimen temperature is 573 K, as shown in Fig. 11. The sample in this case was the same as that for which some results are shown in Fig. 6. Fig. 12 shows I *vs* $1/K^{*2}$ plots for these measurements. It can be seen (Fig. 12) that there is no qualitative change in the nature of the DXS intensity *vs* $1/K^{*2}$ plots even at 573. The slopes of the lines for **K*** along **R*** are still larger than those of the lines for **K*** perpendicular to **R*** (as was observed at room temperature).

Discussion

The description and discussion of the results of DXS measurements at room temperature and higher temperatures have made it abundantly clear that these results cannot be understood in terms of X-ray scattering from elastic thermal waves. The other source of strong DXS close to a relp could be the Huang scattering from point defects. The data obtained with higher-order reflections show that the entire I *vs* $1/K^{*2}$ plot is not a single straight line [Figs. 8(*b*), 9(*b*) and 10(*b*)]. Recently, some investigations of DXS from point-defect aggregates have been reported (Peisl, Spalt

Table 1. *Slopes* (counts cm^{-2}) *of the* I *vs* $1/K^{*2}$ *plots for measurements made around various relps*

	Relp			
K* along	111	333	444	555
[111]	$3{\cdot}1 \times 10^6$	$7{\cdot}4 \times 10^6$	$3{\cdot}14 \times 10^6$	$5{\cdot}1 \times 10^5$
		$2{\cdot}0 \times 10^7$	$1{\cdot}3 \times 10^7$	$4{\cdot}4 \times 10^6$
$[\bar{1}\bar{1}\bar{1}]$	$2{\cdot}1 \times 10^6$	$4{\cdot}4 \times 10^6$	$2{\cdot}4 \times 10^6$	$3{\cdot}5 \times 10^5$
		$1{\cdot}3 \times 10^7$	$8{\cdot}9 \times 10^6$	$4{\cdot}4 \times 10^6$
$[0\bar{1}1]$	$2{\cdot}6 \times 10^4$	$1{\cdot}0 \times 10^6$	$8{\cdot}7 \times 10^5$	$3{\cdot}7 \times 10^5$
		$2{\cdot}1 \times 10^6$	$2{\cdot}7 \times 10^6$	$3{\cdot}3 \times 10^6$
$[01\bar{1}]$	$2{\cdot}4 \times 10^4$	$9{\cdot}1 \times 10^5$	$1{\cdot}4 \times 10^6$	$4{\cdot}2 \times 10^5$
		$2{\cdot}6 \times 10^6$	$3{\cdot}1 \times 10^6$	$3{\cdot}3 \times 10^6$

& Waidelich, 1967; Krivoglaz, 1969; Spalt, 1970; Trinkaus, Spalt & Peisl, 1970; Dederichs, 1973; Patel, 1975). It seems that the DXS observed in the present experiments may be due to aggregates of point defects. We have examined our results bearing in mind these considerations.

If an otherwise perfect crystal contains point-defect aggregates one expects the DXS intensity corresponding to a given $\mathbf{K}^*$ value to be given by the scattering function (Dederichs, 1971):

$$S(\mathbf{H}^*) = \mathrm{UB} \sum_{m,m'} e^{i\mathbf{H}^* \cdot (\gamma_m - \gamma_{m'})} \times (\langle e^{i\mathbf{H}^* \cdot (\mathbf{u}_m - \mathbf{u}_{m'})} \rangle - \langle e^{i\mathbf{H}^* \cdot \mathbf{u}_m} \rangle \langle e^{i\mathbf{H}^* \cdot \mathbf{u}_{m'}} \rangle). \quad (10)$$

Here γ_m is the position of the mth atom in the ideal lattice and $\mathbf{u}_m$ is the static displacement from this position due to the presence of aggregates of point defects. The averages in equation (10) are evaluated for specific models for aggregates of point defects. The distribution of DXS around a relp depends upon the type of defect cluster. For example, Dederichs has shown two entirely different iso-intensity plots for DXS intensity around $h00$ reflections of Cu single crystals for clusters of point defects with three equal crossed dipoles and dislocation loops on {111}. On the basis of these considerations, one excepts an anisotropic distribution of intensity, even for $\mathbf{K}^*$ parallel and antiparallel to a given crystallographic direction. This theory predicts that aggregates of interstitial atoms or ions will have an intensity which is higher for $\mathbf{K}^*$ parallel to $\mathbf{R}^*[\theta > \theta_B]$ than for $\mathbf{K}^*$ antiparallel to $\mathbf{R}^*[\theta < \theta_B]$. The opposite distribution is expected for clusters of vacancies.

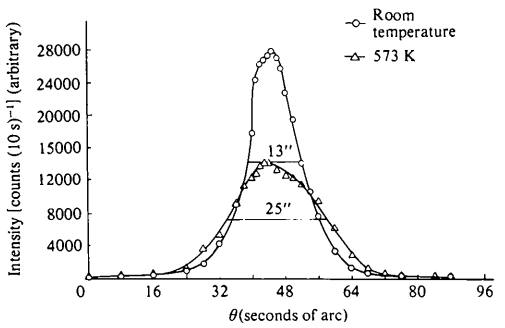

Fig. 11. Diffraction curves obtained for the 111 relp of a (111) dislocation-free Si single crystal at room temperature and 573 K. Cu $K\alpha_1$ radiation was used as the exploring beam.

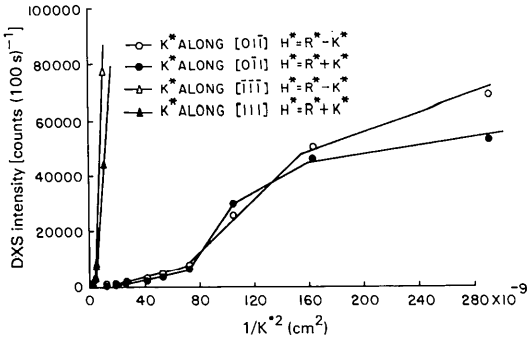

Fig. 12. I *vs* $1/K^{*2}$ plot for the 111 relp of a (111) dislocation-free Si single crystal for DXS measurements made at 573 K. Cu $K\alpha_1$ radiation was used as the exploring beam.

We have plotted all our data of DXS intensity (I) as a function of $\mathbf{K}^*$ on log log graphs. These plots consist of more than one straight line having different slopes. The points where the lines with different slopes meet each other, or knee points, are important parameters. These can give information about the sizes of the point-defect clusters (Dederichs, 1971; Trinkaus, 1972; Patel, 1975). Table 2 gives values of $|\mathbf{K}^*|$ for the different knee points observed in Figs. 4, 6, 8, 9 and 10. It can be seen that the 37 values of $|\mathbf{K}^*|$ (Table 2) corresponding to knee points in Figs. 4, 6, 8, 9 and 10 cover a large range of values. The maximum and minimum have a ratio of 100. However, most of the knee points can be grouped into the following four groups: (1) five knee points with $|\mathbf{K}^*|$ values in the range 2 to 5 $\times 10^3$ cm^{-1}; (2) 21 knee points with $|\mathbf{K}^*|$ values in the range 1 to 3 $\times 10^4$ cm^{-1}; (3) eight knee points with $|\mathbf{K}^*|$ values in the range 5 to 10 $\times 10^4$ cm^{-1}; and (4) three knee points with $|\mathbf{K}^*|$ values $\sim 2 \times 10^5$ cm^{-1}.

This shows that the maximum number of knee points have $|\mathbf{K}^*|$ values in the range 1 to 3 $\times 10^4$ cm^{-1}. This corresponds to a size parameter of about 3000 to 10 000 Å. The observation of knee points with $|\mathbf{K}^*|$ values in four regions may be due to the presence of defect clusters of different sizes.

Recently, we have investigated silicon single crystals which were deliberately treated with oxygen. These crystals were also investigated by infrared absorption and X-ray diffraction topography simultaneously. In

Table 2. *Values of* $|\mathbf{K}^*|$ (cm^{-1}) *at knee points in the* I *vs* $1/K^{*2}$ *plots for measurements made around various relps*

$\mathbf{K}^*$ along	Relp 111	333	444	555
[111]	2.1×10^4	1.3×10^4	1.9×10^4	1.6×10^4
	2.8×10^4	9.5×10^4	1.9×10^5	2.3×10^4
				1.7×10^5
[$\bar{1}\bar{1}\bar{1}$]		3.3×10^4	1.2×10^4	1.6×10^4
			3.1×10^4	4.6×10^4
	2.8×10^4	9.5×10^4	1.9×10^5	8.5×10^4
[01$\bar{1}$]	2.0×10^3	4.8×10^3	1.6×10^4	1.6×10^4
				2.0×10^4
				3.2×10^4
	2.8×10^3	1.3×10^4	6×10^4	7.8×10^4
[0$\bar{1}$1]	2.0×10^3	9.5×10^3	1.6×10^4	1.6×10^4
				3.3×10^4
	4.0×10^3	1.8×10^4	4.6×10^4	5.8×10^4

this case, in DXS intensity plots, the DXS intensity observed for θ greater than θ_B was higher than that for θ less than θ_B. These results suggest the presence of aggregates of interstitial point defects (Lal, Singh, Verma & Schwuttke, 1978), and support the present findings.

Conclusion

Results of these detailed investigations have shown that in silicon single crystals at temperatures at least up to 573 K there is no appreciable contribution of elastic thermal waves to the observed DXS. This is possibly due to the high Debye temperature (640 K) of this material.

The defects gave large scattering near the relps and in the present case most of the defects were of the vacancy type.

The authors are grateful to Dr G. H. Schwuttke for supplying the specimen used in the present investigation.

References

American Institute of Physics Handbook (1957). 3rd ed., pp. 4–116. New York: McGraw-Hill.

BONSE, U. & HART, M. (1965). *Appl. Phys. Lett.* **7**, 238–240.

CHANDRA, S. & HEMKAR, M. P. (1973). *Acta Cryst.* A**29**, 25–28.

DEDERICHS, P. H. (1971). *Phys. Rev. Sect. B*, **4**, 1041–1050.

DEDERICHS, P. H. (1973). *J. Phys. F*, **3**, 471–496.

EISENBERGER, P., ALEXANDROPOULOS, N. G. & PLATZMAN, P. M. (1972). *Phys. Rev. Lett.* **28**, 1519–1522.

JAMES, R. W. (1948). *The Optical Principles of the Diffraction of X-rays*, ch. V, p. 239. London: Bell.

KLUG, H. P. & ALEXANDER, L. E. (1954). *X-ray Diffraction Procedures for Polycrystalline and Amorphous Materials*, p. 272. New York: John Wiley.

KRIVOGLAZ, M. A. (1969). *Theory of X-ray and Thermal Neutron Scattering by Real Crystals*. New York: Plenum.

LAL, K. (1977). Paper presented at the National Conference on Crystallography, Univ. of Madras, Madras, January. [To be published in *Advances in Crystallography*, edited by R. SRINIVASAN. Oxford, New Delhi: IBH Publishing Co.]

LAL, K. & SINGH, B. P. (1977). *Solid State Commun.* **22**, 71–74.

LAL, K. & SINGH, B. P. (1978*a*). *Indian J. Phys.* In the press.

LAL, K. & SINGH, B. P. (1978*b*). To be published.

LAL, K., SINGH, B. P. & VERMA, A. R. (1978). Paper presented at the IVth International Conference on Vapour Growth and Epitaxy, Nagoya, Japan, July 9–13.

LAL, K., SINGH, B. P., VERMA, A. R. & SCHWUTTKE, G. H. (1978). XIth International Congress of Crystallography, Warszawa, Poland, August 3–12. Abstract No. 11.5–12.

LARSEN, B. C. & SCHMATZ, W. (1974). *Phys. Rev. Sect. B*, **10**, 2307–2314.

PATEL, J. R. (1975). *J. Appl. Cryst.* **8**, 186–191.

PEISL, H. (1975). *J. Appl. Cryst.* **8**, 143–149.

PEISL, H., SPALT, H. & WAIDELICH, W. (1967). *Phys. Status Solidi*, **23**, K75.

PHATAK, S. D., SRIVASTAVA, R. C. & SUBBARAO, E. C. (1972). *Acta Cryst.* A**28**, 227–231.

PRASAD, S. C. & WOOSTER, W. A. (1955). *Acta Cryst.* **8**, 361.

RAMACHANDRAN, G. N. & WOOSTER, W. A. (1951*a*). *Acta Cryst.* **4**, 335–344.

RAMACHANDRAN, G. N. & WOOSTER, W. A. (1951*b*). *Acta Cryst.* **4**, 431–440.

SPALT, H. (1970). *Z. Angew. Phys.* **29**, 269.

SPALT, H., LOHSTOLER, H. & PEISL, H. (1973). *Phys. Status Solidi B*, **56**, 469–482.

TRINKAUS, H. (1972). *Phys. Status Solidi B*, **51**, 307–319.

TRINKAUS, H., SPALT, H. & PEISL, H. (1970). *Phys. Status Solidi A*, **2**, K97.

WALKER, C. B. (1956). *Phys. Rev.* **103**, 547–557.

WOOSTER, W. A. (1962). *Diffuse X-ray Reflections from Crystals*. Oxford: Clarendon Press.